An Experimental Study of Bubble Departure Diameter in Subcooled Flow Boiling Including the Effects of Orientation Angle, Subcooling, Mass Flux, Heat Flux, and Pressure

R. Sugrue[a], J. Buongiorno, T. McKrell

Massachusetts Institute of Technology, Department of Nuclear Science and Engineering, 77 Massachusetts Avenue, Cambridge, MA, USA
[a] *rsugrue@mit.edu, +1-617-253-7522*

Abstract

The effects of orientation angle, subcooling, heat flux, mass flux, and pressure on bubble departure diameter in the isolated bubble regime of subcooled flow boiling were studied by high-speed video in a two-phase flow loop that can accommodate a wide range of flow conditions. Specifically, the following ranges were explored: orientation angles of 0° (downward-facing horizontal), 30°, 45°, 60°, 90° (vertical), and 180° (upward-facing horizontal); mass flux values of 250, 300, 350, and 400 kg/m^{2}s, corresponding to Froude numbers between 0.42 and 1.06; pressures of 101 (atmospheric), 202, and 505 kPa; two values of the subcooling degrees (10 and 20°C); and two heat fluxes (0.05 and 0.10 MW/m^2). The combination of the test section design, high-speed video camera and LED lighting results in high accuracy (order of 20 microns) in the determination of the bubble departure diameter. The data indicate that the bubble departure diameter increases with increasing heat flux, decreasing mass flux, decreasing subcooling, and decreasing pressure. Also, the bubble departure diameter increases with decreasing orientation angle, i.e. the largest bubbles are found to detach from a downward-facing horizontal surface. The mechanistic bubble departure diameter model of Klausner et al. and its recent modification by Yun et al. were found to correctly predict all the observed parametric trends, but with large average errors and standard deviation: 65.5±75.8% for Klausner's and 37.9±51.2% for Yun's. Since the cube of the bubble departure diameter is used in subcooled flow boiling heat transfer models, such large errors are clearly unacceptable, and underscore the need for more accurate bubble departure diameter models.

1. Introduction

Understanding and predicting the complex phenomena involved in two-phase flow and boiling heat transfer is necessary for the efficient operation, safety, and development of light-water cooled reactors. In U.S. Pressurized Water Reactor (PWR) plants, subcooled flow boiling occurs in the hot fuel assemblies under normal operating conditions, and determines the margin to Critical Heat Flux (CHF) (Kazimi and Todreas 1990). Subcooled flow boiling also determines the rate at which corrosion products in solution in the coolant deposit on the surface of the zircaloy cladding, which can lead to localized corrosion and neutronic distortions (axial offset), and ultimately cladding failure.

The state-of-the-art simulation approach for nuclear systems with two-phase flow and heat transfer relies on CFD simulations implementing the Eulerian-Eulerian, two-fluid, six-equation model (Bestion et al. 2009, In and Chun 2009, Lo et al. 2011, Michta et al. 2011) with or without an interfacial area transport model (Ishii and Hibiki 2006). Such approaches require closure relations for the phase-to-phase and wall-to-flow mass, momentum, and energy terms in the governing equations. Subcooled boiling heat transfer is captured by the wall-to-flow constitutive relation for energy. Examples of boiling heat transfer constitutive relations are the heat flux partitioning model of Kurul and Podowski (1990), Kolev's bubble interaction model (2002), and the more recent hybrid numerical-empirical model of Sanna et al. (2009). All these models require accurate knowledge of the bubble departure diameter. For example, in the partitioning heat flux model, heat removal by the boiling fluid is assumed to be through three contributions, (i) the latent heat of evaporation to form the bubbles (q''_e), (ii) heat expended in re-formation of the thermal boundary layer following bubble departure, or the so-called quenching heat flux (q''_q), and (iii) heat transferred to the liquid phase outside the zone of influence of the bubbles by

convection (q"$_c$). The total boiling heat flux is then obtained as the sum of the three fluxes:

$$q'' = q''_e + q''_q + q''_c \quad (1)$$

The latent heat flux is often the dominant term in Eq. 1, and can be written as:

$$q''_e = \frac{\pi}{6} D_b^3 \rho_v h_f f_b n'' \quad (2)$$

where D_b is the bubble departure diameter, f_b is the frequency of bubble departure, n'' is the nucleation site density, ρ_v and h_{fg} are the vapor density and latent heat of evaporation, respectively. The cubic dependence in Eq. 2 suggests that small uncertainties on the bubble departure diameter are greatly magnified in the heat transfer model, thus deteriorating the accuracy of the overall CFD simulation. Therefore, using robust and accurate bubble departure models is key to the successful prediction of subcooled flow boiling heat transfer.

2. Previous Work & Motivation

High-speed digital photography has been utilized extensively to study bubble characteristics in a variety of flow boiling contexts. Thorncroft et al. (1998) experimentally investigated vapor bubble growth and detachment processes for vertical upflow as well as downflow boiling under slightly subcooled conditions utilizing high-speed digital imagery to assess bubble size, growth rate, bubble departure and lift-off diameter, and waiting time from isolated nucleation sites. The studies were conducted for FC-87 refrigerant over a nichrome heating surface with mass flux ranging from 190 to 666 kg/m^{2}s and heat flux from 1.3 to 14.6 kW/m^2. Results indicated that the bubble characteristics associated with upflow and downflow boiling are significantly different, with upflow bubble dynamics leading to higher heat transfer coefficient due to sliding of the bubbles. Bibeau (1994) also used high speed imaging, and found that bubbles continued growing as they slide along the heating surface until reaching a maximum size at which the condensation rate equals the evaporation rate. Gerardi et al. (2010) used synchronized digital imaging and infrared thermometry to simultaneously measure the growth rate and thermal footprint of steam bubbles in pool boiling. Situ et al. (2005) conducted a series of studies in forced convective subcooled flow boiling of water under vertical upflow in an annulus, using a high-speed digital camera to assess bubble lift-off diameters, growth rate, and velocity after lift off. Data were taken at atmospheric pressure with mass flux values between 466 to 900 kg/m^{2}s and heat flux in the range of 54 to 206 kW/m^2. The data suggested a strong dependence of the bubble departure frequency on the wall heat flux. Basu et al. (2002), in a series of investigations of upward-vertical subcooled flow, assessed waiting time, bubble growth time, and bubble departure size for water on two heaters with different surface finish. The heat flux and wall superheat required for boiling inception were found to be dependent on flow rate, liquid subcooling, and contact angle of the surface. Subsequently, Situ and colleagues (2008) determined bubble departure characteristics, such as bubble departure frequency, lift-off diameter, and growth rate, for 58 test conditions in a vertical upflow annular channel with water as the working fluid. Tests were run at atmospheric pressure with inlet temperature ranging from 80°C to 98°C and heat flux from 60.7 to 206 kW/m^2 utilizing a high-speed digital camera to capture bubble nucleation. They used their data to develop a correlation for bubble lift-off diameter as a function of Jakob number and Prandtl number, which reproduces the data well at low wall superheat. Euh et al. (2010) investigated bubble nucleation in vertical forced-convective subcooled boiling upflow for water under varying pressures from 167 to 346 kPa, mass fluxes ranging from 214 to 1869 kg/m^{2}s, and heat fluxes from 61 to 238 kW/m^2. Results indicated that bubble departure frequency increased with heat flux and pressure but decreased with increasing mass flux and degree of subcooling. This was consistent with Situ et al. findings (modifying the Situ et al. empirical equation for higher atmospheric pressures), but was not congruent with the Basu et al. data collected under lower mass flux and higher heat flux conditions. A number of other experimental and analytical studies have investigated various fluids and channel geometries, as well as pressure, degree of subcooling, and flow rate ranges, to develop and validate models predicting bubble parameters,

particularly bubble size at detachment (Yeoh and Tu 2005, Yun et al. 2010, Yun et al. 2012, Wu et al. 2008, Chen et al. 2009).

The most commonly-used mechanistic bubble departure model for flow boiling is that of Klausner et al. (1993), which is based on a balance of static and dynamic forces for the bubble throughout its growth cycle. Klausner postulates that at the time of departure that balance is broken and the bubble can either lift off (non-zero force perpendicular to the wall) or slide along the wall (non-zero force tangential to the wall). This model was originally calibrated to predict bubble departure size in refrigerant R113 flow. Subsequently, Zeng et al. (1993) modified and expanded the applicability of the Klausner's model for both horizontal and vertical channels under pool and flow boiling conditions with refrigerant R113, with pressure ranging from 20 to 280 kPa; Jakob number between 4 and 869; and gravity 1 to 0.014 g. Situ et al. (2005) and Yeoh et al. (2005) extended the model to flow conditions with water, and Yun et al. (2010, 2012) recently improved the model's predictive capability by incorporating a bubble condensation model as well as evaluating the model for a wider range of pressure, temperature, and flow rates.

None of the studies referenced above have thoroughly investigated the impact that the orientation angle of the channel has on bubble departure diameter. In high mass flux situations, which are typical of full-power reactor operation, the Froude number is high, thus the effects of buoyancy forces and channel orientation can be neglected (Celata and Mariani 1999). However, when the mass flux is lower, buoyancy forces and channel orientation are expected to be important. This is the case in applications such as current reactors under off-normal operations (e.g., natural circulation following loss of flow, or decay heat removal from the vessel surface during severe accidents, the so-called in-vessel retention), in small modular reactors using natural circulation under normal operation, and in electronic cooling applications.

Furthermore, while many of the experimental studies noted above used high-speed video or photographic visualization techniques to measure bubble diameter, most were conducted in a vertical or horizontal annulus with an interior heating mechanism, which makes it difficult to image the bubbles growing at the wall clearly. Few of these designs have utilized the high spatial resolution of advanced cameras, which is needed to generate high-accuracy data for validation of constitutive models in CFD codes.

3. Objectives & Innovations

The primary objective of this study is to investigate the effects of mass flux, heat flux, degree of subcooling, pressure and angle of orientation of the heater surface on the departure diameter of steam bubbles in the isolated bubble regime of subcooled flow boiling. The test matrix is shown in Table 1. The values of the mass flux were chosen sufficiently low to ensure a significant effect of the orientation angle, as suggested by Klausner's model. The corresponding range of Froude number (based on the channel hydraulic diameter) is 0.42 to 1.06, and range of Reynolds number is 11800 to 34500. The heat flux range was chosen to ensure that subcooled flow boiling occurs in the so-called 'isolated bubbles' regime, where interactions between bubbles at adjacent nucleation sites can be neglected. The ranges for the other parameters were chosen to produce measurable changes of the bubble departure diameter, within the operating envelop of our facility.

The main novelty of this database is the systematic investigation of the effect of the orientation angle on bubble departure diameter in subcooled flow boiling, and the high level of accuracy (tens of microns) in the measurement of the bubble departure diameter, achieved through the combination of the high-speed camera, LED lighting and special optical design of the test section used in our facility.

Table 1. Experimental test matrix.

Parameter	**Units**	**Experimental Range**
Orientation Angle:	[°]	0, 30, 45, 60, 90, 180
Mass Flux:	[kg/m^{2}s]	250, 300, 350, 400
Subcooling:	[°C]	10, 20
Heat Flux:	[MW/m^2]	0.05, 0.10
Pressure:	[kPa]	101, 202, 505

4. Experimental Setup

4.1 Flow Loop & Test Section Description

The primary components of the flow loop include a pump (Grundfos centrifugal pump, model A97518318-P10943121, max 58.4 L/min), pre-heater (2-kW immersion), test section, accumulator (Blacoh CT2420V bladder-style design), condenser (Thermasys heat shell-and-tube exchanger), DC power supply (max 30 V, 600 A), Nitrogen gas tank, measurement instrumentation (various thermocouples, pressure, volumetric flowrate, current and voltage taps), and a data acquisition system with LabVIEW software. A schematic of the loop is shown in Figure 1. All wetted metallic components are made of type 316L stainless steel.

The test section consists of a rectangular stainless steel (316L) body, two viewing windows (front and back), a heater, and a Macor insulator. The heater is flat, 1 cm wide by 24 cm long, made of 316L and fits into the Macor ceramic insulator, which acts as both an electrical and thermal insulator. The receding and advancing contact angles of water on the heater surface at room temperature are 8° and 91° respectively, as measured with a goniometer, and the surface roughness is 1.22 μm. The rectangular flow channel through the test section body has a width of 1.43 cm, a depth of 1.99 cm, a length of 31.75 cm, and an equivalent diameter of 1.67 cm. Figure 2 shows a schematic of the full test section assembly. Copper studs, used as connections to the power supply lines that provide DC current, are screwed into the ends of the heater. Eight thermocouples are screwed into the back of the test section and touch the back of the heater to acquire temperature readings throughout the experiments. The test section is connected to the loop by a stainless steel reinforced flexible (viton) tube and a 90° elbow compression fitting, thus its orientation can be adjusted to any angle from 0° (downward facing) to 90° (vertical upflow) to 180° (upward facing).

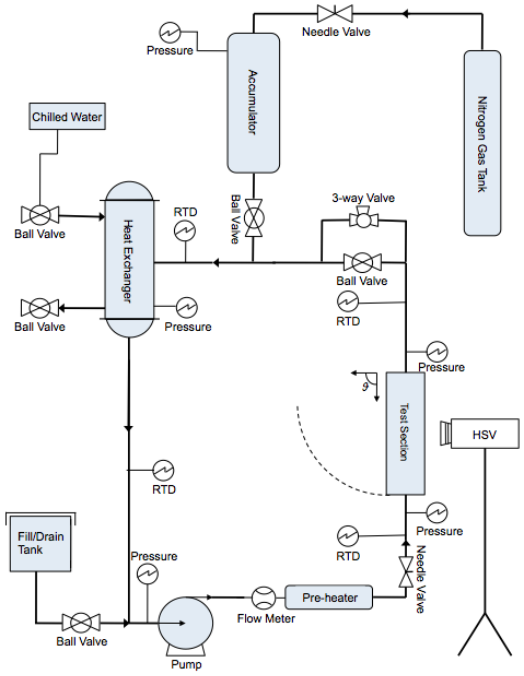

Fig. 1. Schematic of the flow loop. The test section orientation angles are measured from the horizontal, downward-facing reference position (0°).

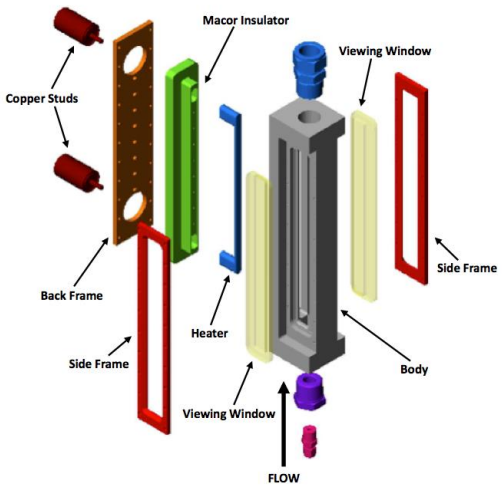

Fig. 2. Schematic of the test section assembly.

A Phantom V12 high-speed video camera is used to measure the bubble departure diameter during the experimental runs. The camera has an image size of 1280x800 pixels and is capable of capturing images at a rate of 6242 fps at full image size and up to 10^6 fps for a reduced number of pixels per image size. Three Digital Promaster Nikon extension rings (12mm, 20mm, and 36mm) are used to increase the magnification with a 200mm Nikon lens. Two Lowell DC LED

lights are used as direct backlighting during the experiments. They provide sufficient light for the desired camera acquisition rate and avoid the flickering associated with AC, one of the typical problems associated with high-speed video for clear visualization (Gerardi et al. 2010).

4.2 Experimental Procedure & Estimated Uncertainties

To initiate the experiments, the test section is adjusted at the desired orientation angle. About 10 liters of de-ionized water are added to the fill tank and heated up to ~60°C using a 1-kW immersion heater. The fill tank is pressurized using the Nitrogen gas tank (pressure uncertainty is ±0.25% of full range) and water is pushed into the pre-evacuated loop. Once the loop is water tight, the pump and power supplies are turned on and the preheater is used to help raise the bulk fluid temperature. Degassing is done at ~60°C, by allowing non-condensable gases to exit the loop into the fill tank through a degassing line on the top side of the loop. Successful degassing is verified with an oxygen probe and is completed once no bubbles are released through the degassing line. Once the bulk fluid reaches ~80°C, fine adjustments are made using the preheater and chilled water system to maintain the desired degree of subcooling (within ±0.5°C). The subcooling is then decreased by adjusting chilled water flow and preheater power, and the heat and mass flux are easily adjusted according to the test matrix. The uncertainty on the measured heat flux and mass flux is ±1% and ±2%, respectively.

A single nucleation site is chosen approximately one third of the way up the heater and is used for the range of parameters in the experimental matrix. High-speed videos are recorded for ten bubbles from that same nucleation site at each set of operating conditions. The images taken with the high-speed video were all captured at a frame rate of 5000 fps with an image size of 1280x800 pixels. All the bubbles imaged in this work are near-perfectly spherical, however values for diameter are determined to be an average of the longest and shortest lengths of the bubble. The bubble departure diameter is the diameter of the bubble measured at the instant (frame) in which the bubble detaches from the surface. The uncertainty on the diameter of a single bubble is one pixel or ±0.019 mm, as measured with respect to a reference reticule. The wall temperature at the nucleation site of interest is obtained from the wall thermocouple readings, corrected for conduction heat transfer through the heater. The estimated uncertainty for the wall temperature is ±1°C.

5. Results

Figure 3 shows consecutive images of a single bubble starting from its initial growth through to departure. Tables 2 and 3 show the bubble departure diameter data for the full test matrix at atmospheric pressure and elevated pressures, respectively. The measured wall temperatures at the nucleation site of interest are also reported in Tables 2 and 3. Figure 4 shows images of representative bubbles at the time of departure from heaters at 90°, 45° and 0° orientation angle, respectively, with 10°C subcooling, heat flux of 0.05 MW/m^2 and various mass fluxes.

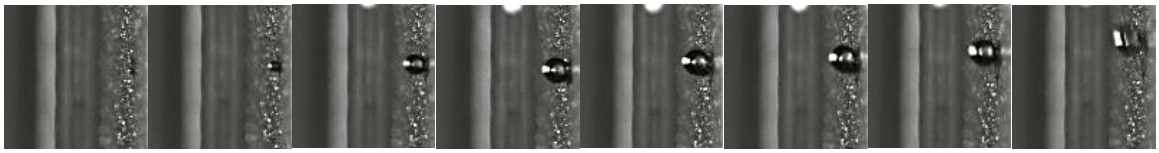

Fig. 3. Consecutive images of a bubble from its initial growth to its departure.

Table 2. Summary of experimental results at atmospheric pressure. The first line in each row presents the bubble departure diameters and their related uncertainty, defined as the root sum square of the systematic and random uncertainty. The second line shows the measured wall temperature in °C at the nucleation site of interest. Pressure is given in kPa, subcooling is given in °C, heat flux in MW/m^2, mass flux in kg/m^{2}s, and diameters in mm. The uncertainty on the values of the wall temperature is ±1°C. At this pressure (atmospheric), the saturation temperature of water is 100°C, so 20°C subcooling reflects a bulk temperature of 80°C, and 10°C subcooling reflects a bulk of 90°C.

P	AT_{sub}	q"	G	0°	30°	45°	60°	90°	180°
			250	0.615±0.032	0.552±0.027	0.514±0.089	0.471±0.021	0.371±0.021	0.581±0.103
				102°	102°	102°	102°	102°	102°
			300	0.528±0.024	0.446±0.025	0.421±0.115	0.391±0.021	0.295±0.021	0.330±0.027
		0.05		102°	102°	102°	102°	102°	102°
			350	0.429±0.020	0.375±0.021	0.377±0.103	0.333±0.021	0.267±0.019	0.316±0.027
				102°	102°	102°	102°	102°	102°
			400	0.389±0.026	0.322±0.021	0.325±0.040	0.299±0.021	0.229±0.019	0.265±0.027
	20°			102°	102°	102°	102°	102°	102°
			250	0.632±0.035	0.598±0.029	0.532±0.071	0.497±0.024	0.381±0.019	1.000±0.092
				105°	104°	105°	105°	104°	104°
			300	0.560±0.034	0.444±0.034	0.439±0.036	0.389±0.031	0.324±0.027	0.754±0.064
		0.10		104°	104°	105°	105°	104°	104°
			350	0.453±0.049	0.392±0.026	0.399±0.041	0.356±0.021	0.267±0.027	0.570±0.068
				104°	104°	104°	104°	104°	104°
			400	0.434±0.038	0.337±0.026	0.331±0.048	0.286±0.024	0.248±0.027	0.377±0.036
101 kPa				104°	105°	104°	104°	104°	104°
			250	0.623±0.039	0.581±0.055	0.538±0.098	0.457±0.036	0.362±0.019	0.518±0.089
				103°	103°	103°	103°	103°	103°
			300	0.503±0.038	0.453±0.028	0.478±0.097	0.379±0.026	0.314±0.021	0.511±0.065
		0.05		103°	103°	103°	103°	103°	103°
			350	0.432±0.027	0.381±0.028	0.405±0.073	0.345±0.026	0.295±0.021	0.459±0.085
				103°	103°	103°	103°	103°	103°
			400	0.370±0.038	0.345±0.025	0.349±0.053	0.301±0.025	0.248±0.019	0.406±0.056
	10°			103°	103°	103°	103°	103°	103°
			250	0.668±0.072	0.625±0.063	0.519±0.070	0.463±0.028	0.391±0.021	0.600±0.115
				106°	106°	106°	106°	106°	106°
			300	0.518±0.055	0.490±0.053	0.427±0.046	0.358±0.027	0.352±0.021	0.529±0.058
		0.10		106°	106°	106°	106°	106°	106°
			350	0.440±0.046	0.394±0.035	0.373±0.050	0.333±0.021	0.305±0.019	0.420±0.045
				106°	106°	106°	106°	106°	106°
			400	0.358±0.027	0.324±0.024	0.333±0.036	0.305±0.023	0.267±0.019	0.355±0.043
				106°	106°	106°	106°	106°	106°

Table 3. Summary of experimental results for elevated pressures and a downward-facing horizontal (0°) heater. The first line in each row presents the diameters (and related uncertainty), and the second line shows the measured wall temperature in °C at the nucleation site of interest. Subcooling is given in °C, heat flux in MW/m^2, mass flux in kg/m^{2}s, and diameters in mm. The uncertainty on the values of the wall temperature is ±1°C. At a pressure of 202 kPa, the saturation temperature of water is 118°C, so 20°C subcooling reflects a bulk temperature of 98°C, and 10°C subcooling reflects a bulk of 108°C. For a pressure of 505 kPa, the saturation temperature is 152°C, so 20°C subcooling reflects a bulk temperature of 132°C, and 10°C subcooling reflects a bulk of 142°C.

ΔT_{sub}	q"	G	P = 202 kPa	P = 505 kPa
		250	0.573±0.053	0.262±0.029
			119°	153°
		300	0.456±0.076	0.192±0.029
	0.05		119°	153°
		350	0.357±0.043	0.166±0.035
			119°	153°
		400	0.337±0.049	0.160±0.033
20°			120°	153°
		250	0.605±0.059	0.413±0.025
			120°	155°
		300	0.533±0.067	0.290±0.028
	0.10		120°	155°
		350	0.427±0.053	0.261±0.021
			120°	155°
		400	0.387±0.029	0.224±0.022
			120°	155°
		250	0.419±0.031	0.282±0.031
			122°	155°
		300	0.373±0.030	0.255±0.026
	0.05		122°	155°
		350	0.322±0.040	0.231±0.027
			122°	155°
		400	0.320±0.044	0.194±0.027
10°			122°	155°
		250	0.511±0.067	0.326±0.037
			122°	157°
		300	0.384±0.048	0.288±0.025
	0.10		123°	157°
		350	0.357±0.033	0.278±0.024
			123°	157°
		400	0.322±0.042	0.236±0.027
			123°	157°

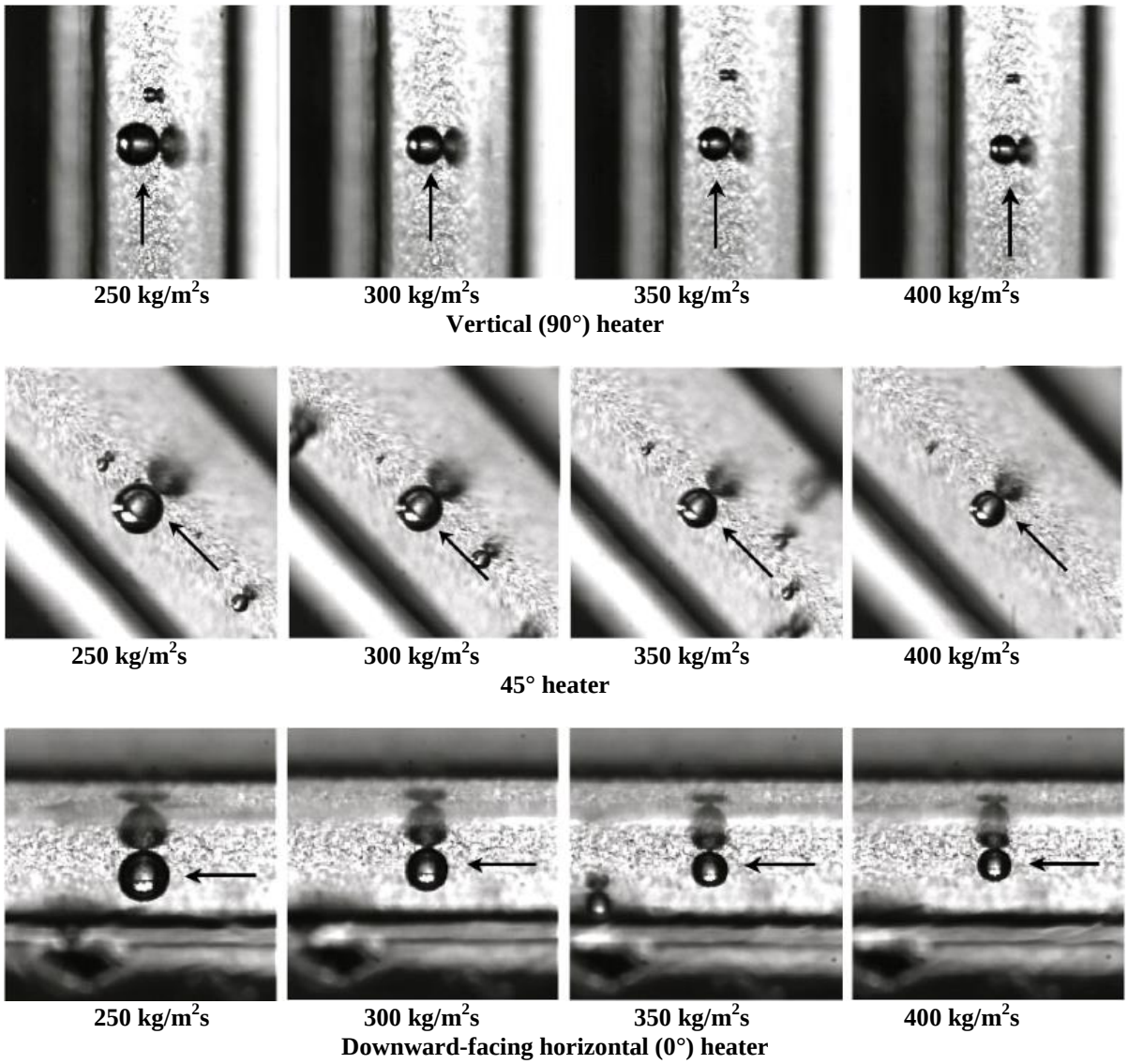

Fig. 4. Images of bubbles at the moment of departure as functions of mass flux and orientation angle. The degree of subcooling is 10°C and the heat flux is 0.05 MW/m^2 for all images.

6. Discussion

As can be seen from the tables and images in the previous section, the bubble departure diameter increases with increasing heat flux, decreasing mass flux, decreasing subcooling, and decreasing pressure. All these trends are expected. Briefly, a higher mass flux increases the drag force, which accelerates bubble departure. A higher heat flux increases the rate of bubble growth resulting in larger bubbles at departure. Higher pressure translates into smaller bubbles because of the higher density of the vapor. Higher subcooling limits the size of the bubbles via condensation. Finally, as the bubble departure mode in these tests is sliding (vs lifting off), the bubble departure diameter reaches a minimum at an orientation angle of 90° (vertical), because the tangential component of the buoyancy force is largest at that angle.

Figures 5, 6, and 7 show plots of selected data vs. orientation angle, mass flux, and pressure, respectively, along with the predictions of Klausner's model (Klausner et al. 1993) and Yun's modified version of Klausner's model (Yun

et al. 2010), implemented by ad-hoc Matlab scripts[1]. Both models correctly reproduce the experimentally observed trends, but systematically overpredict the data. Error distribution curves for the whole database are shown in Figure 8. It is clear from this graph that Yun's model predicts the experimental data more accurately than Klausner's original model. The bulk of the data is predicted with errors below 50% by both models, but the data points above this are from the models' predictions for a downward-facing horizontal (0°) heater. Specifically, the average error and standard deviation for Klausner's model is 65.5±75.8%, while for Yun's model is 37.9±51.2%. Note that such inaccuracies in the bubble departure diameter prediction would translate into very large errors (100-180%), if propagated in a mechanistic model of boiling heat transfer like Eq. 2, because of the cubic dependence.

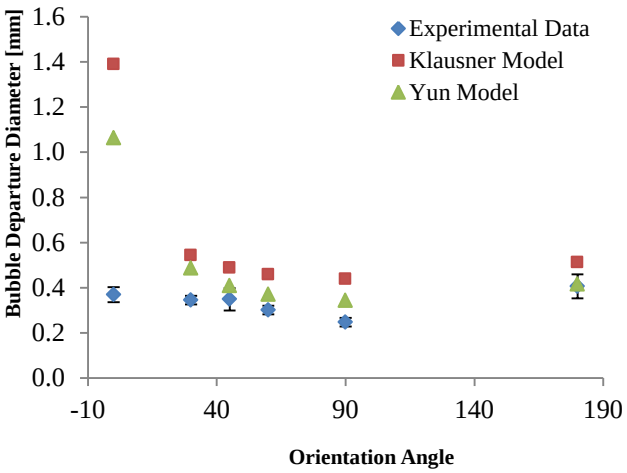

Fig. 5. Comparison between Klausner's original model predictions, Yun's modified model, and experimental data for bubble departure diameter as a function of orientation angle; 10°C subcooling, 0.05 MW/m^2, 400 kg/m^{2}s, atmospheric pressure.

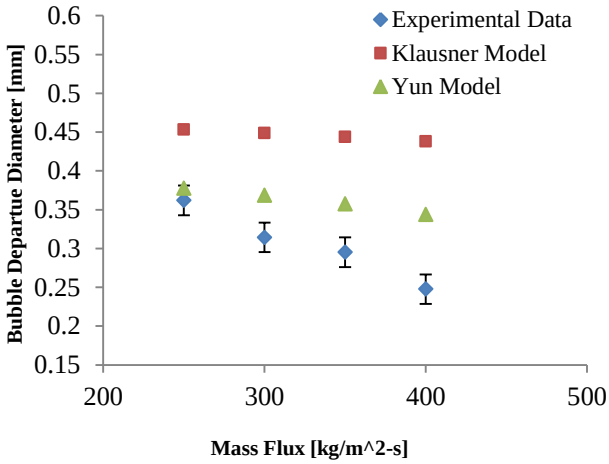

Fig. 6. Comparison between Klausner's original model predictions, Yun's modified model, and experimental data for bubble departure diameter as a function of mass flux; vertical (90°) heater, 10°C subcooling, 0.05 MW/m^2, atmospheric pressure.

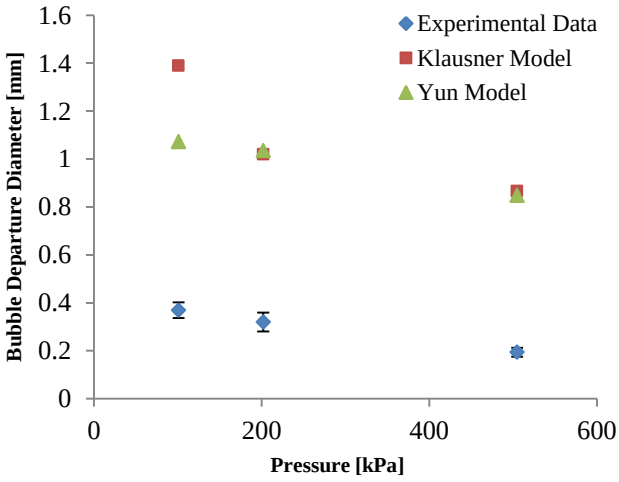

Fig. 7. Comparison between Klausner's original model predictions, Yun's modified model, and experimental data for bubble departure diameter as a function of pressure; downward-facing horizontal (0°) heater, 10°C subcooling, 0.05 MW/m^2, 400 kg/m^{2}s.

[1] The experimentally measured subcooling was used in the model of Yun.

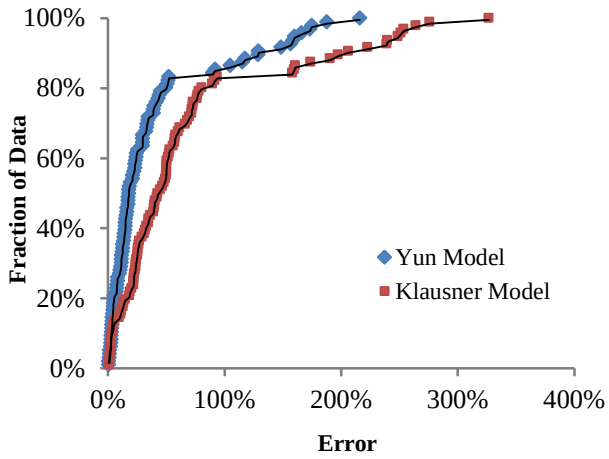

Fig. 8. Error distributions for Klausner's and Yun's models. The long tails of the distributions represent the data for the downward-facing horizontal heater.

7. Conclusions

The effects of orientation angle, subcooling, heat flux, mass flux, and pressure on bubble detachment in subcooled flow boiling were experimentally investigated and compared to predictions from two bubble departure models, Klausner's mechanistic model and Yun et al.'s modification to Klausner's model. The predicted and experimentally observed relationships between these parameters and bubble departure diameter are in good qualitative agreement. However, the models systematically overpredict the data with large overall error statistics, i.e. 65.5±75.8% for Klausner's model and 37.9±51.2% for Yun's model.

Ongoing work focuses on improving the accuracy of Klausner's and Yun's models in predicting bubble departure diameter at PWR normal and off-normal conditions. To that end, the dominant force terms in the models are being identified for the PWR conditions. Then the models for those forces will be trained/calibrated with the experimental data presented in this paper. Finally, the improved bubble departure model will be used in CFD simulations of the PWR hot channel, where subcooled flow boiling occurs.

Nomenclature

D_b	Bubble departure diameter
f_b	frequency of bubble departure
h_{fg}	latent heat of evaporation
n''	nucleation site density
q_c	condensation heat flux
q_e	evaporation heat flux
q_q	quenching heat flux
q_{tot}	total heat flux
ρ	density

Subscripts

l	liquid phase
v	vapor phase

Acknowledgements

Ms. Sugrue's studies at MIT are supported by a National Academy for Nuclear Training (NANT) fellowship. The authors also wish to express their gratitude to Mr. Doug Spreng for his financial support, and Lowell Lighting LLC for donating the LED lights used in the experiments. In addition, special thanks to Dr. Greg DeWitt for designing and building the experimental loop used in this research, as well as Eric Forrest and Bren Phillips for their assistance throughout the experimental runs.

References

M. Kazimi, N. Todreas. 1990. *Nuclear Systems I: Thermal Hydraulics Fundamentals* Taylor and Francis Group, LLC.

D. Bestion et al., Some lessons learned from the use of Two-Phase CFD for Nuclear Reactor Thermalhydraulics, N13-P1139, Proc. of NURETH-13, Kanazawa, Japan, September 27-October 2, 2009.

W. K. In and T.-H. Chun, CFD Analysis of a Nuclear Fuel Bundle Test for Void Distribution Benchmark, N13-P1259, Proc. of NURETH-13, Kanazawa, Japan, September 27-October 2, 2009.

S. Lo, A. Splawski and B. J. Yun, The Importance of Correct Modeling of Bubble Size and Condensation in Prediction of Sub-Cooled Boiling Flows, Paper # 75, NURETH-14, Toronto, Ontario, Canada, September 25-30, 2011.

E. Michta, K. Fu, H. Anglart and K. Angele, Numerical Predictions of Bubbly Two-Phase Flows

with Openfoam, Paper # 617, NURETH-14, Toronto, Ontario, Canada, September 25-30, 2011.

M. Ishii, T. Hibiki. 2006. *Thermo-fluid Dynamics of Two-phase Flow*, Springer.

N. Kurul, M.Z. Podowski. 1990. Multidimensional effects in forced convection subcooled boiling, *Proc. 9th International Heat Transfer Conference*, Jerusalem, Israel. pp. 21-25.

N. Kolev. 2002. How accurately can we predict nucleate boiling?, *Multiphase Flow Dynamics 2*, Springer.

A. Sanna, C. Hutter, D.B.R. Kenning, T.G. Karayiannis, K. Sefiane, R.A. Nelson. 2009. Nucleate Pool Boiling Investigation on a Silicon Test Section with Micro-Fabricated Cavities, *ECI International Conference on Boiling Heat Transfer*, Florianopolis, Brazil, May 3-7.

G.E. Thorncroft, J.F. Klausner, R. Mei. 1998. An experimental investigation of bubble growth and detachment in vertical upflow and downflow boiling. *International Journal of Heat and Mass Transfer*, Vol. 41, 3857-3871.

E.L. Bibeau, M. Salcudean. 1994. A study of bubble ebullition in forced-convective subcooled nucleate boiling at low pressure. *International Journal of Heat and Mass Transfer*, Vol. 37, pp. 2245-2259.

C. Gerardi, J. Buongiorno, L. Hu, T. McKrell, 2010. Study of bubble growth in water pool boiling through synchronized, infrared thermometry and high-speed video. *International Journal of Heat and Mass Transfer*, Vol. 53, 4185-4192.

R. Situ, T. Hibiki, M. Ishii, M. Mori. 2005. Bubble lift-off size in forced convective subcooled boiling flow; *International Journal of Heat and Mass Transfer*, 48 (2005) 5536-5548.

N. Basu, G.R. Warrier, V.K. Dhir. 2002. Onset of nucleate boiling and active nucleation site density during subcooled flow boiling. *J. Heat Transfer*, Vol. 124, pp. 717-728.

R. Situ, M. Ishii, T. Hibiki, J.Y. Tu, G.H. Yeoh, M. Mori. 2008. Bubble departure frequency in forced convective subcooled boiling flow. *Int. J. of Heat and Mass Transfer*, Vol. 51, pp. 6268-6282.

D. Euh, B. Ozar, T. Hibiki, M. Ishii, C. Song, 2010. Characteristics of bubble departure frequency in a low-pressure subcooled boiling flow. *J. Nuc. Science and Tech*., Vol. 47, No. 7, 608-617.

G.H. Yeoh, J.Y. Tu. 2005. A unified model considering force balances for departing vapour bubbles and population balance in subcooled boiling flow; *Nuclear Engineering and Design* 235 (2005) 1251-1265.

B.J. Yun, A. Splawski, S. Lo, C.-H. Song. 2010. Advanced Wall Boiling Model for the Subcooled Boiling Flow with CFD Code; *The Seventh Korea-Japan Symposium on Nuclear Thermal Hydraulics and Safety*, Chuncheon, Korea, November 14-17.

B.J. Yun, A. Splawski, S. Lo, C.-H. Song. 2012. Prediction of a subcooled boiling flow with advanced two-phase flow models; *Nuclear Engineering and Design* 253(2012) 351-359.

W. Wu, P. Chen, B.G. Jones, T.A. Newell. 2008. A study of bubble detachment and the impact of heated surface structure in sub cooled nucleate boiling flows; *Nuclear Engineering and Design* 238(2008) 2693-2698.

C.A. Chen, W.R.Chang, K.W. Li, Y.M.Lie, T.F. Lin. 2009. Subcooled flow boiling heat transfer of R-407C and associated bubble characteristics in a narrow annular duct, *Int. J. of Heat and Mass Transfer*, 53(2009) 3147-4158.

J.F. Klausner, R. Mei, D.M. Bernhard, Z. Zeng. 1993. Vapor bubble departure in forced convection boiling; *Int. J. of Heat and Mass Transfer*, Vol. 36. No. 3. pp. 651-662, 1993.

L.Z. Zeng, J.F. Klausner, D.M. Bernhard, R. Mei. 1993. A unified model for the prediction of bubble detachment diameters in boiling systems – II. Flow boiling; *Int.l J. of Heat and Mass Transfer*, Vol. 36, No. 9, pp. 2271-2279, 1993.

G.P. Celata, A. Mariani, 1999. CHF and post-CHF heat transfer, in *Handbook of phase change, boiling and condensation*. Kandlikar, S.G. et al (Eds), NY: Taylor and Francis, pp. 443-493.

H. Kolev. 2011. Bubble departure diameter. *Multiphase Flow Dynamics 3: Thermal Interactions*, Springer.